

## SANS from Surfactant-Treated Nylon Fibres

S.M. King<sup>1</sup>, D.G. Bucknall<sup>2</sup>, and R.K. Heenan<sup>1</sup>

[1] Large Scale Structures Group, ISIS Facility, Rutherford Appleton Laboratory, Chilton, OX11 0QX, UK

[2] Department of Materials, University of Oxford, Parks Road, Oxford, OX1 3PH, UK

Received 9th December 2003; accepted in revised form 16th March 2004

### ABSTRACT

*We report preliminary results from a Small Angle Neutron Scattering (SANS) study of nylon rope fibres treated with environmental contaminants of the type that the fibres may experience in everyday use.*

### Introduction

Modern high performance ropes are no longer made from siseal or hemp but from synthetic polymers such as nylon-6 (e.g. Perlon®, Ultramid B®, Zytel PA®, and Akulon®), nylon-6/6, polyesters, polypropylene, high-modulus polyethylene (e.g. Dyneema® or Spectra®), aramids (e.g. Twaron® or Kevlar®), and more recently even liquid crystalline polymers (e.g. Vectran®).

Another major difference is in the construction of the rope. Natural fibre ropes have traditionally been hawserlaid (or plaited), but modern synthetic fibre ropes have a kernmantel construction in which a core bundle (the "kern") of coiled yarns is encased in a woven outer sheath (the "mantle"), free to slip against the core (Figure 1).

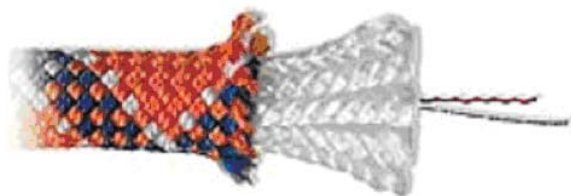


**Figure 1.** The internal construction of a modern synthetic rope. © Edelrid GmbH. For scale the diameter of the sheath is about 10mm. On the right are marker and tracer threads. In this rope the sheath houses 14 strands, each coiled from 3 yarns. Each yarn contains many single fibre filaments.

The actual type of fibre and the degree of coiling and arrangement (plaited together or not) of the core yarns determines the energy absorption capability of the rope (through the degree of extension under load) and thus to a large extent determines the mechanical properties as well. Ropes that extend more are called "dynamic" or "climbing" ropes, and those that extend less are called "static", "caving" or "abseil" ropes. These two types of rope are used in very different situations. Indeed, if a person were to shock load a static rope (e.g. as might happen in a fall) it would very likely prove fatal.

In kernmantel ropes the load handling capability is also partitioned between the core and the sheath. Some manufacturers also offer combination ropes in which the core

and sheath are different polymer fibres. This allows the performance of the rope to be matched to particular applications.

Whilst the condition of the sheath is clearly easy to establish, the same is not true of the core fibres. Contemporary methods of rope testing are reliant on destructive mechanical tests (and it has been said that the interpretation of some of the data often leave a great deal to be desired).

### Background

One of the major problems with synthetic fibre ropes is the degree to which environmental factors affect the chemical stability of the fibres. Nylons, for example, are degraded by UV radiation (e.g. sunlight), and are chemically attacked by acids (such as might leak from a miner's or cavers lead-acid battery). The mechanical test data even indicate that water affects the physical properties of the fibres (Figure 2). Soiled ropes present

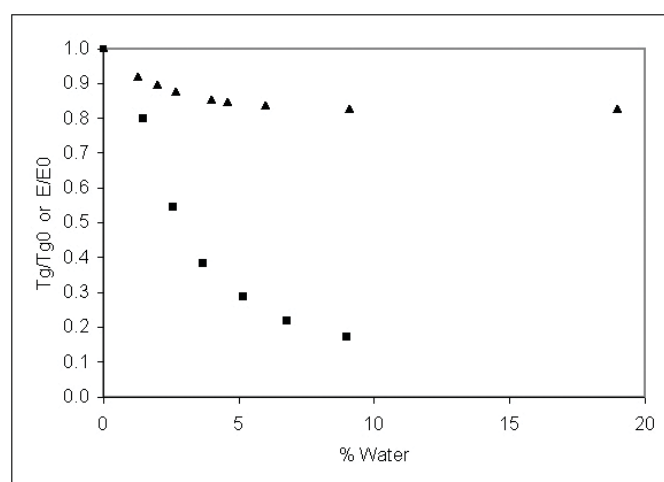


**Figure 2.** The relative variation of the glass transition temperature  $T_g$  (▲) and Young's modulus  $E$  (■) of nylon-6 with the degree of hydration. Data taken from References [1], [2] & [3].

another worry, that of how best to clean them. Even though the fibres are essentially the same as those used in textile manufacture, there is conflicting evidence about the wisdom of

using commercial detergent formulations and fabric conditioners on synthetic fibre ropes.

Tests conducted in a study by Smith [4] indicate that treatment with concentrated fabric conditioner reduced the strength (breaking load) of new rope in dynamic tests. Frank [5] showed that certain ropes treated with dilute conditioner (as per the manufacturer's recommendations) were actually stronger than the same rope without conditioning, after ageing and wear. Frank proposed that the likely mechanism at work explaining these results was that the fibre lubricants present in new rope are lost with age, allowing the fibres to cut one another. The addition of fabric conditioner then replaces some of the lubricants, but excess quantities effectively leave the rope fibres wet, with a corresponding loss in strength (as depicted in Figure 2).

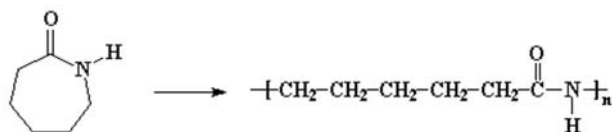
With this mechanism in mind, a further argument for treatment with fabric conditioner would be its effect on the "Hookean spring constant" of the rope. Since the spring constant would be determined by both the properties of the nylon fibre and the weave, it is likely that conditioner will offset premature stiffening due to the loss of internal lubricants.

Given that ropes actually have a significant part to play in modern life (and life styles) - for example, the now infamous Millennium Dome in London was "roofed" by a team of Rope Access Technicians, and each year hundreds of thousands of people worldwide trust their lives to the integrity of their ropes whilst climbing and potholing - there is clearly a need for a more rigorous scientific understanding of some of these phenomena.

There might also be considerable interest from rope manufacturers and users alike if a non- or less-destructive rope-testing regimen could be devised.

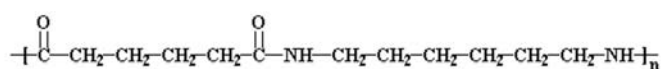
## Nylons

Nylon-6 is made by a ring opening polymerisation of  $\epsilon$ -caprolactam (1-aza-2-cycloheptanone):



The polymer is therefore also known as polycaprolactam, polyamide-6 (PA-6) or poly[imino(1-oxo-1,6-hexanediy)]].

Note that this is a very different polymer to nylon-6/6 (PA-66), patented by Dupont in the 1940's and often made in school chemistry lessons, which has become synonymous with the colloquial term *nylon*. PA-66, made by condensation polymerisation of adipic acid (hexanedioic acid) and hexamethylene diamine (1,6-hexanediamine), is:



A comparison of some physical properties of nylon-6 and nylon-6/6 are given in Table 1.

Property	Nylon 6	Nylon 6/6
Density (g/cm <sup>3</sup> )	1.12 - 1.14	1.09 - 1.14
T <sub>glass</sub> (°C)	47 - 57	35 - 78
T <sub>softening</sub> (°C)	200	243
T <sub>melting</sub> (°C)	210 - 223	255 - 280
Yield stress (MPa)	40 - 90	60 - 98
Yield strain (%)	16 - 7	18 - 4.5
Elongation (%)	260 - 70	250 - 46
Tensile modulus (MPa)	1300 - 3500	1700 - 3300
Water absorption (%)	10	8.5

**Table 1. Some physical properties of nylon-6 and nylon-6/6. Where a range is given for mechanical data, the former figure refers to 50% Relative Humidity and the latter to the dry state. Data are predominantly taken from the Polymer Data Handbook, Reference [6].**

Fibres are formed from the polymer in a two-step process involving melt-spinning and drawing. It is the drawing (though a 100  $\mu\text{m}$  orifice at perhaps 100  $\text{ms}^{-1}$ ) that imparts molecular orientation and modifies the crystallinity of the fibres [7].

The crystallographic structure and morphology of nylon-6 have been extensively studied. No fewer than *four* monoclinic crystal phases (denoted  $\alpha$ ,  $\alpha'$ ,  $\beta$ , and  $\gamma$ ) have been reported [8, 9, 10, 11]. The  $\alpha'$ -phase is a high-temperature phase, the existence of which has been taken as evidence of a Brill transition in nylon-6. There is also evidence of a fifth, triclinic, phase (denoted  $\lambda$ ) but this has so far only been observed in nylon-6 oligomers [12, 13]. In the thermodynamically stable  $\alpha$  phase and in the  $\beta$  phase, hydrogen bonds form between neighbouring, all-trans ("ribbon-like"), *antiparallel* chains. The chains are directed along the *c*-axis and the hydrogen bonds parallel to the *a*-axis. This gives rise to flat sheets in the *ac*-plane. In the  $\alpha$ -phase adjacent sheets are separated by a repeat distance of  $\Delta b = 1.724$  nm and interdigitated ("sheared") parallel to the *a*-axis by  $\Delta c \leq 0.21$  nm (perhaps around 0.14 nm). In the  $\gamma$ -phase sheets of hydrogen-bonded chains are also present but with several notable differences. The secondary amide groups are twisted out of the *ac*-plane by  $66^\circ$  (giving the  $\gamma$ -phase a "twisted-helical" conformation) and this allows hydrogen bonding to take place between neighbouring *parallel* chains. The separation of the sheets is slightly smaller,  $\Delta b = 1.688$  nm, and the direction of the chains also reverses in alternating sheets.

The significance of these structures to the present contribution is that nylon-6 fibre production has a tendency to promote the formation of the kinetically favoured  $\gamma$ -phase over the  $\alpha$ -phase, but because melting and recrystallisation can convert  $\gamma \rightarrow \alpha$  both are usually present in the final fibre (the ratio depending on the actual processing conditions).

In contrast, nylon-6/6 has *three* triclinic crystal phases (denoted  $\alpha_1$ ,  $\alpha_2$ , and  $\beta$ ) but no  $\gamma$  phase. There is however a high-temperature form of the  $\alpha_1$  phase which is monoclinic. The  $\beta$  phase is only formed during high-temperature annealing in a vacuum. The structures of the  $\alpha$  and  $\beta$  phases are analogous to those in nylon-6, but because the nylon-6/6 unit cell is centrosymmetric there is no concept of parallel and antiparallel chains, the two arrangements are equivalent.

The above is, however, not a complete description of the fibre structure because the lamellar sheets are not of infinite length. Each fibre actually consists of finite sections of crystalline lamellae (the "sheets" discussed earlier) joined by equivalently finite sections of amorphous polymer to form what is termed a "lamellar stack" (Figure 3). Nylons are thus *semi-crystalline* polymers. The crystallinity of a lamellar stack is 70 - 80%, but the overall crystallinity of a fibre is perhaps only 45 - 50%.

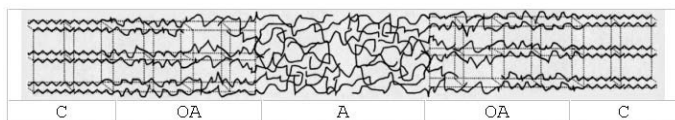


**Figure 3. Idealised schematic representation of the arrangement and different types of polymer chain conformations in a lamellar stack. Key: C = crystalline, OA = oriented amorphous, A = amorphous. Adapted reprint from Reference [17]. Copyright (2002), with permission from Elsevier.**

The amorphous polymer (along with a small contribution from thermal diffuse scattering from the ordered polymer) gives rise to an amorphous halo in the scattering pattern, the position and width of which varies with the degree of orientation in the fibre and changes in the density of the amorphous regions. In an unoriented nylon-6 fibre sample this halo occurs at a  $d \sim 0.42$  nm ( $Q \sim 14.96$  nm<sup>-1</sup>) [15, 18]. In an oriented fibre it has been shown that the amorphous polymer also has preferential orientation [15, 19], some chains align parallel to the chain axis, others align perpendicular to the chain axis. The former are more " $\alpha$ -like", the latter are more " $\gamma$ -like".

A useful overview of the structural characterisation of nylon-6 has recently been given by Rieger [20]. The hierarchy of the fibre structure is summarised in Figure 4.

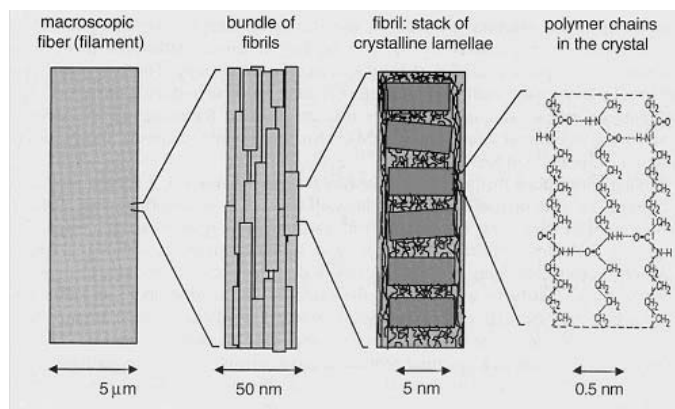


**Figure 4. The hierarchical structure of a nylon-6 fibre. The locations of the inter-lamellar and inter-fibrillar amorphous polymer are clearly visible. Reprinted from Reference [20]. Copyright (2002), with permission from Elsevier.**

## Previous Work

It is the very presence of the regions of amorphous (non-crystalline) polymer in the fibre that actually mediate many of the physical and mechanical properties conferred on the fibre by the crystalline polymer. Of particular interest in this work is the fact that the solvation of nylon fibres proceeds by diffusion of solvent molecules into the amorphous regions. From here a proportion of these solvent molecules probably also diffuse between the lamellae in the crystalline regions. It is this incorporation of solvent that gives rise to the sort of reversible effects depicted in Figure 2, as intercatenary hydrogen bonds are replaced by interactions with water molecules [3]. On average, one water molecule is associated with every amide (-CONH-) linkage in the amorphous regions [21].

There is a significant body of work on the mechanisms and molecular consequences of the hydration of nylon-6 by Murthy and co-workers [21, 22, 23, 24, 25] and others [26] using techniques such as SAXS, WAXS, SANS, INS, IR/Raman and <sup>2</sup>D-NMR. Murthy [25] also compared solvation by water with that by ethylene glycol (a "stronger" solvent known to affect the properties of nylons).

The NMR data show two types of "bound" water and a more mobile form. This is interpreted as evidence of partitioning between the lamellar stacks and the inter-fibrillar domains. One, perhaps surprising, observation is that it appears as much as two-thirds of the amorphous chains lie outside of the lamellar stacks. There is also evidence that water and other small solvent molecules can diffuse directly through the fold surfaces of the crystalline lamellae.

When fibres of different draw ratio (degree of orientation) are compared it is found that the amount of water in the inter-fibrillar domains remains quite constant, whereas that in the inter-lamellar regions decreases. This suggests that the amount of amorphous polymer in the inter-fibrillar regions remains unchanged during the drawing process and, in turn, suggests that the increases in crystallinity are due to amorphous chains in the inter-lamellar region being incorporated into the lamellae.

In contrast, the available literature concerning the effects of the adsorption of surfactants by nylon is, to all intents and purposes, non-existent (though there are some examples relating to the adsorption of dyes and proteins/DNA). However, this may in part be for reasons of commercial confidentiality.

## Why Neutron Fibre Diffraction?

Though X-ray fibre diffraction is of course a well-established, high-flux, high-resolution technique, it is not actually very well suited to the aims of the present study. For example:

- since the amount of adsorption of surfactants onto/into the fibres will not be particularly high it is not sufficient to examine a handful of treated fibres with a  $\mu$ m-sized beam, an element of bulk averaging is required;
- even synchrotron X-ray beams struggle to pass through a polymer sample more than 1 mm thick, or contained in a cuvette filled with solvent;
- ionic surfactants contain high-Z counterions which will dominate the underlying scattering from the polymer;
- non-ionic surfactants, being composed of atoms of similar Z to the polymer, will exhibit little electron density difference ("contrast").

Neutron beams on the other hand are typically collimated to several mm in size (a natural consequence of the larger source) and are highly-penetrating (in a brief test that we conducted it proved possible to measure a SANS pattern from a *whole* 8 mm diameter nylon kernmantel rope). In addition, by exploiting <sup>2</sup>D for <sup>1</sup>H substitution it is possible to selectively manipulate the contrast, or to effectively remove the contribution to the scattering of some components. The drawback with neutron fibre diffraction is the relative lack of flux that puts data collection times on current sources into the range of minutes to

hours and therefore rules out the sort of *in-situ* kinetic studies (e.g. cold drawing, simultaneous DSC) that are possible with X-rays.

Perhaps because of this there are very few examples of *neutron* diffraction from synthetic polymer fibres. The work on nylon-6 (cited above) and Tencel® (a cellulosic fibre) [27] are thus significant in this regard. Neutron diffraction from *biological* fibres (e.g. DNA) is much more widely established because of its ability to locate coordinated water.

## Instrumentation

Small- and wide-angle neutron diffraction data were simultaneously collected on the LOQ instrument at the ISIS Spallation Neutron Source, Chilton, Oxfordshire, UK [28]. This is a fixed-geometry, "white beam", instrument that utilises time-of-flight techniques on neutrons with wavelengths between 0.2 and 1 nm to provide a continuous and simultaneous  $Q$ -range of 0.06 - 14 nm<sup>-1</sup> (where  $Q$  is the modulus of the scattering vector) [29]. LOQ has two 2D position-sensitive detectors that overlap in  $Q$ -space. The incident beam was collimated to a circular cross-section of 8 mm diameter or a rectangular slit 8mm (H) x 2mm (W).

Each raw scattering dataset was corrected for the sample transmission and background scattering, detector efficiency and linearity, and converted to scattering cross-section data ( $\partial\Sigma/\partial\Omega$  versus  $Q$ ) using the instrument-specific software [30]. The reduced data are placed on an absolute scale using a well-characterized solid blend of hydrogenous and perdeuterated polystyrene as a calibrant [31].

## Experimental

Yarns approximately 3 cm in length were extracted from the core of a metre length of Edelrid Superstatic® static kernmantel rope. The rope had previously been soaked in pure water for 10 days (to remove the sizing used in manufacture) and then dried at room temperature whilst hanging under their own weight for a further 8 days. Samples of these yarns were then soaked in:

- deuterium oxide, **D<sub>2</sub>O**, (as a control);
- a 20 wt% solution of sodium deuterioxide, **NaOD**, in D<sub>2</sub>O;
- 11 wt% and 33 wt% solutions of perdeuterated sulphuric acid, **D<sub>2</sub>SO<sub>4</sub>**, in D<sub>2</sub>O;
- a 13 cmc solution of the *anionic* surfactant perdeuterated sodium dodecyl (or lauryl) sulphate, **dSDS** (CH<sub>3</sub>(CH<sub>2</sub>)<sub>11</sub>SO<sub>4</sub><sup>-</sup>Na<sup>+</sup>), in D<sub>2</sub>O;
- a 13 cmc solution of the *cationic* surfactant perdeuterated hexadecyl (or cetyl) trimethyl-ammonium bromide, **dC<sub>16</sub>TAB** (CH<sub>3</sub>(CH<sub>2</sub>)<sub>15</sub>N<sup>+</sup>(CH<sub>3</sub>)<sub>3</sub>Br<sup>-</sup>), in D<sub>2</sub>O;
- a 13 cmc solution of the *non-ionic* surfactant perdeuterated hexaethyleneglycol mono-dodecyl ether (or 6 lauryl ether), **dC<sub>12</sub>E<sub>6</sub>** (CH<sub>3</sub>(CH<sub>2</sub>)<sub>11</sub>(OCH<sub>2</sub>CH<sub>2</sub>)<sub>6</sub>OH), in D<sub>2</sub>O.

where *cmc* refers to the critical micelle concentration. The deuterium oxide, sodium deuterioxide, sulphuric acid and dSDS were obtained from Aldrich Chemical Co. Ltd. The dC<sub>16</sub>TAB and dC<sub>12</sub>E<sub>6</sub> were gifts from Dr I. Tucker of Unilever Research. The rationale behind the selection of chemical treatment was as follows. The alkali solution is of equivalent strength to the

electrolyte found in a Ni-Fe cell (battery), whilst the stronger of the two acid solutions is of equivalent strength to the electrolyte found in a Pb-acid cell. Both types of cell are used by miners, cavers and potholers. In addition it is well known that polyamides undergo acid-catalysed hydrolysis of the amide linkage. Hence samples treated with the two different strength acid solutions were expected to show different degrees of degradation. This would in turn allow the sensitivity of the study to be evaluated. Finally, cationic and non-ionic surfactants are the major constituents (typically 10 - 20%) of commercial washing powders and fabric conditioners. Anionic surfactants are sometimes also present.

Some measurements were also made with samples soaked in "*null scattering water*" (a mixture 8.7 wt% D<sub>2</sub>O : 91.3 wt% H<sub>2</sub>O that has a neutron scattering length density,  $\rho$ , of zero and thus does not scatter neutrons) and "*contrast match water*" (a mixture 21.8 wt% D<sub>2</sub>O : 78.2 wt% H<sub>2</sub>O that has a neutron scattering length density equal to the average of that for crystalline, 0.91x10<sup>10</sup> cm<sup>-2</sup>, and amorphous, 0.80x10<sup>10</sup> cm<sup>-2</sup>, nylon-6 [22]; that is  $\rho = 0.85x10^{10}$  cm<sup>-2</sup>). To a very good approximation the scattering length densities of nylon-6 and nylon-6/6 are the same.

Two types of sample mounting were used. In our earlier experiments the yarns were placed in 1 mm path length quartz cuvettes. Initially two-part cuvettes of the "dish-and-cover slip" variety were used. These allowed something of the macroscopic alignment of the fibres to be maintained in the beam, but unfortunately made it difficult to keep the fibres fully hydrated over the period of data collection (~2 hrs) as the cells were not leak-tight. Consequently a second set of measurements as made with the yarns tamped into conventional rectangular (but un-necked) cuvettes that were then filled with the relevant solution and sealed with PTFE plumber's tape. This "small-angle scattering" approach is not by any means an optimum arrangement, is certainly unconventional (in the X-ray sense), and could not be expected to yield discrete Bragg peaks because of the orientational averaging. It is nonetheless perfectly valid. The scattering from cuvettes only filled with the different solutions as also recorded and subtracted from the fibre scattering. This also removed the inherent instrumental background scattering.

Later experiments utilised a "fibre holder" made in-house (Figure 5). Mounted on a goniometer cradle on top of a rotation stage, this not only ensured that the macroscopic alignment of the yarns was standardised but, if desired, the moveable clamps permitted an extensional strain to be applied. To maintain relative humidity a small dish of D<sub>2</sub>O was placed under the yarn before the holder was encased by a box cover with aluminium foil beam entry/exit windows.

## Results and Discussion

Representative (except for the case of 33 wt% D<sub>2</sub>SO<sub>4</sub>) radially averaged (0° - 360°) scattering data are shown in Figure 6. Several features are apparent. At very low- $Q$  there is quite intense scattering that decays rapidly (from ~ 100 cm<sup>-1</sup> at  $Q = 0.06$  nm<sup>-1</sup> in the case of the D<sub>2</sub>O data shown) with increasing  $Q$ . This scattering has a power law dependence of  $\sim Q^{-3.9}$ , suggesting that it arises from surface scattering from the fibrils.

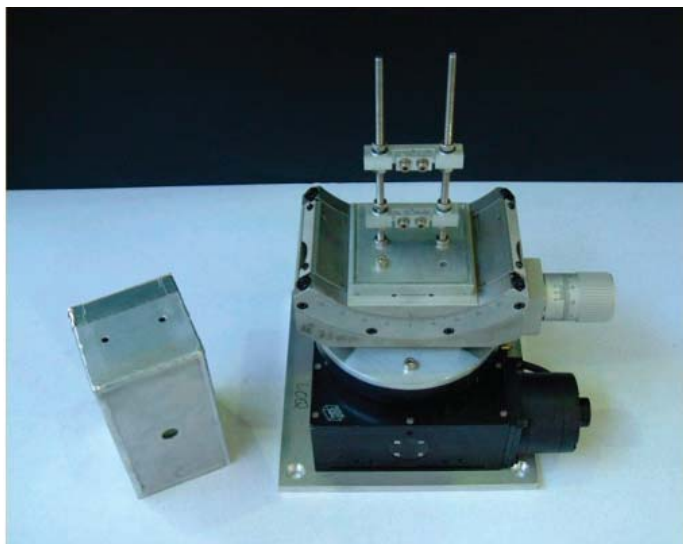


Figure 5. The fibre holder employed in later SANS experiments. The ends of the yarn are clamped between the two cross-pieces. On the left is the cover that maintains humidity around the sample. The beam entry hole is visible on the front surface. A laser beam directed along the neutron flight path allowed the sample to be positioned accurately on the beam line.

Superimposed on this power law decay is a broad diffraction peak centred on  $Q \sim 0.76 \text{ nm}^{-1}$ ; a repeat distance of  $\sim 8.3 \text{ nm}$ . This has been identified as the Long Period,  $L$ , arising from the separation of the crystalline and amorphous regions in the lamellar stacks [21, 26]. The crystalline lamellae are  $\text{D}_2\text{O}$ -deficient in the hydrated fibres, whereas the amorphous regions are  $\text{D}_2\text{O}$ -rich. There is thus a regularly repeating pattern of low and high neutron scattering length density in each stack. When this contrast difference is negligible, as in dry fibres or fibres hydrated in "null" or "contrast match" water, the Bragg peak all but disappears. The width of the peak clearly reflects a broad distribution of repeat distances within the lamellar stacks. Thus the crystalline and amorphous regions are not all of the same length, and neither are the stacks (fibrils).

Finally, at higher  $Q$  values, there is a much weaker and very broad peak apparently centred on  $Q \sim 8.5 \text{ nm}^{-1}$ . This could, at least in part, be evidence of the [020] reflection from the monoclinic unit cell of nylon-6. The higher order crystalline reflections are beyond the detection limit of the LOQ instrument being between  $14 < Q (\text{nm}^{-1}) < 17$  [14, 15, 16].

To extract the Long Period data for the different samples a  $Q^{-3.9}$  power law background was first subtracted from the data to reduce the skewing of the peak. The resulting data are then fitted to a Cauchy function using the CCP13 *XFIT* program [32]

Treated with:	$L$ (nm)	$\Delta Q$ ( $\text{nm}^{-1}$ )	Treated with:	$L$ (nm)	$\Delta Q$ ( $\text{nm}^{-1}$ )
Month 1			Month 41		
$\text{D}_2\text{O}$	8.61	0.71	-	-	-
dSdS	8.73	0.67	dSdS	7.76	0.74
dC16TAB	8.98	0.85	-	-	-
dC12E6	8.38	0.68	dC12E6	8.17	0.54
NaOD	8.06	0.65	NaOD	7.80	0.81
11%D2S04	8.61	0.66	11%D2S04	9.00	0.53
33%D2S04	21.7	0.42	-	-	-

Table 2: Summary of the structural data derived from peak fitting analysis. Key:  $L$  = Long Period,  $\Delta Q$  = peak width.

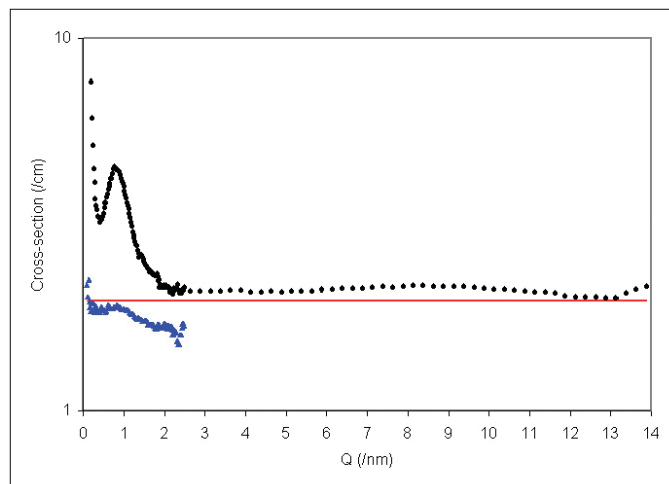


Figure 6. The small- and wide-angle scattering from static fibres hydrated with  $\text{D}_2\text{O}$  ( $\blacklozenge$ ). The  $Q$ -resolution of the two detector banks is different and this gives rise to the change in spacing between data points. An arbitrary baseline has also been added in order to emphasise the feature at high- $Q$ . Also shown for comparison (cross-section  $\times 2$ ) is the small-angle scattering from the same fibres hydrated with "contrast match water" ( $\blacktriangle$ ).

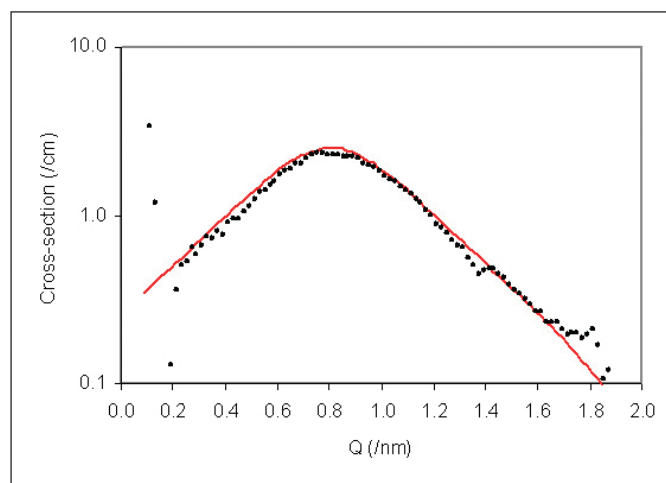
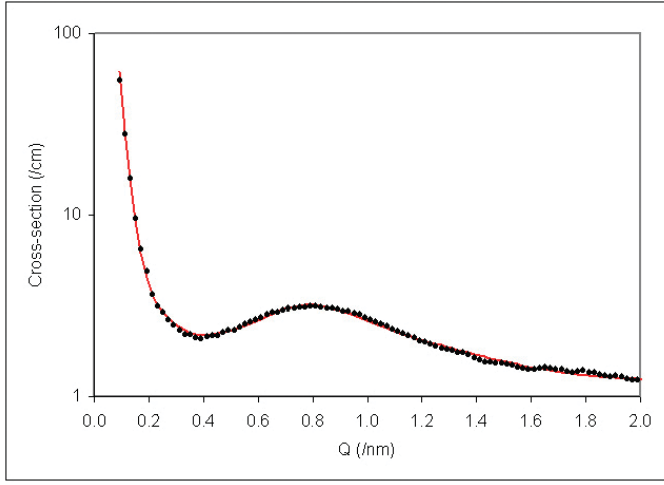


Figure 7. The small-angle scattering from static fibres hydrated with  $\text{D}_2\text{O}$  after subtraction of the underlying surface scattering ( $\blacklozenge$ ), together with a Cauchy peak fit.

(Figure 7).

The Bragg peaks in the data from the dry fibres, and those hydrated with "null water" and  $\text{H}_2\text{O}$ , were too weak to be fitted with any reliability. The Long Period data are given in Table 2.

The drawback with this type of peak fitting analysis is that the information it can provide is necessarily limited. A more rigorous approach would be to fit as much of the scattering as possible to a representative model. The one-dimensional "paracrystal" model of Kotlarchyk & Ritzau [33] is one such description. When coupled with a  $Q^{-4}$  background function this gives a good description of the scattering from the fibres, see Figure 8.



**Figure 8.** The small-angle scattering from static fibres exposed to 11 wt%  $D_2SO_4$  (◆) together with a paracrystal model-fit assuming an "idealised" lamellar structure (see text).

Two variants of the paracrystal model were tested against the scattering data. In the first, the separation and thickness of the lamellar regions were assumed to be constant; i.e. the model was one of an "idealised" lamellar structure. In the second variant, the separation and thickness of the lamellae were both allowed to randomly vary within a Gaussian distribution of length scales (but the scattering length density profiles were still sharp-sided; no allowance was made for "transition regions" between the crystalline lamellae and amorphous polymer). During the fitting the scattering length densities of the crystalline polymer and bulk medium were fixed at their known values; i.e. it was assumed that solvent could only penetrate the amorphous regions.

The former model proved more sensitive to the repeat distance and number of lamellae, but not to the thickness of the lamellae. The latter model was more sensitive to the thickness of the lamellae and solvent penetration into the amorphous regions, but not to the number of lamellae.

A comparison of the information derived from such fits is shown in Table 3. The fits were performed using the *FISH* model-fitting program written by one of the present authors [34].

	$D_2O$	11% $D_2SO_4$
	"idealised"	
Number of lamellae	5-6	4-5
Thickness, T (nm)	2.99	3.04
$\sigma_T / T$	0.05	0.05
Long Period, L (nm)	6.78	6.73
$\sigma_L / L$	0.35	0.35
	"Gaussian"	
Number of lamellae	<20	<10
Thickness, T (nm)	2.68	2.85
$\sigma_T$ (nm)	1.09	0.97
Long Period, L (nm)	5.99	5.98
$\sigma_L$ (nm)	2.19	2.24
$\phi_{polymer}$	0.29	0.24

**Table 3.** Comparison of the structural data derived from example paracrystal model fits to the scattering from static fibres.  $\phi_{polymer}$  is the composition of the amorphous region derived from the scattering length density term included in the "Gaussian" model.

The scattering from fibres exposed to the 33 wt%  $D_2SO_4$  solution is rather different (Figure 9). It is more intense, and the Long Period has increased by such a large extent that the diffraction peak is now a shoulder on the low- $Q$  decay. There is also a complete absence of structure at higher  $Q$  values. This should not, perhaps, be too surprising since the fibres in this sample had been rather seriously degraded. It is nonetheless reassuring to see that such changes are reflected in the scattering. Initially the scattering decays as  $Q^{-1.1}$  to  $Q^{-1.5}$  then, after the shoulder, as  $Q^{-2.2}$  to  $Q^{-2.6}$ . This is completely different behaviour to that exhibited by the other samples, even those treated with 11 wt%  $D_2SO_4$ . Another method of analysing

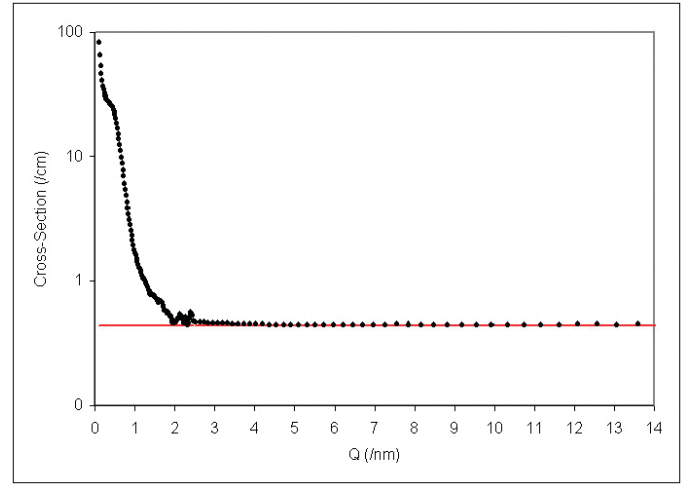


**Figure 9.** The small- and wide-angle scattering from static fibres exposed to 33 wt%  $D_2SO_4$  (◆). An arbitrary baseline has also been added. The apparent features around  $Q \sim 2 \text{ nm}^{-1}$  are at the limit of the low-angle detector and are not statistically significant.

scattering patterns from a system with a regular spacing is to calculate the one-dimensional correlation function,  $\Gamma_1(z)$  [35], from which a wide variety of structural characteristics can be inferred.  $\Gamma_1(z)$  is given by the expression:

$$\Gamma_1(z) = \int_0^\infty \frac{d\Sigma}{d\Omega}(Q) Q^2 \cos(Qz) dQ / \int_0^\infty \frac{d\Sigma}{d\Omega}(Q) Q^2 dQ$$

Note that the denominator in the above is identical with the so-called Invariant Integral,  $Q^*$ . This contains information about the composition of, and scattering length density difference between, the different phases. Given the length scales being investigated in this work, and the fact that the underlying surface scattering has been subtracted, the lamellar stacks can be treated as being just two-phase; crystalline polymer ("c") and hydrated amorphous polymer ("a"). Thus [36]

$$\begin{aligned} Q^* &= 2\pi^2 (\rho_c - \rho_a^{eff}) \phi_{stacks} \omega_c (1 - \omega_c) \\ &= 2\pi^2 (\rho_c - \rho_a^{eff}) \phi_c (1 - \omega_c) \end{aligned}$$

where  $\rho$  is the scattering length density,  $\omega_c$  is termed the local crystallinity, and  $\phi_c$  is the *volume* or *bulk* crystallinity. These last two parameters are derived from analysis of the relevant correlation functions. We note in passing that Crawshaw *et al* [27] have used a three-phase variant of the above expression to consider the system TENCEL fibres / air-filled voids / water. The effective scattering length of the hydrated amorphous

polymer can be used to estimate the volume fraction of solvent,  $\phi_{sol}$ , present since

$$\rho_a^{eff} = (1 - \phi_{sol})\rho_a + \phi_{sol}\rho_{sol}$$

Correlation functions were generated using the CCP13 *CORFUNC* program after Guinier or Vonk (low- $Q$ ) and sigmoidal (high- $Q$ ) extrapolations respectively. The latter is essentially a Porod function modified to allow for a finite width ( $\sqrt{F}$ ) at the boundary between the crystalline and amorphous regions [37].

$$\frac{d\Sigma}{d\Omega}(Q \rightarrow 0) = A \exp(-BQ^2) \quad \text{Guinier}$$

$$\frac{d\Sigma}{d\Omega}(Q \rightarrow 0) = C - DQ^2 \quad \text{Vonc}$$

$$\frac{d\Sigma}{d\Omega}(Q \rightarrow \infty) = \frac{E}{Q^4} \exp(-FQ^2) + G \quad \text{Sigmoid}$$

Here  $A$  and  $E$  are scalars related to the number concentration of fibrils,  $B$  is related to the size of the fibrils, and  $G$  is the residual (principally incoherent) background. The calculated  $\Gamma_1(z)$  functions are shown in Figure 10.

It is immediately apparent that the microstructure of the nylon fibres appears unaffected by treatment with any of the surfactant solutions. But the same cannot be said of those fibres treated with acid or alkali. Some of the parameters derived from these correlation functions are given in Tables 4 and 5. Reassuringly, there is good agreement with the model-fit data in Table 3.

Treated with:	$L$ (nm)	$l_c$ (nm)	$l_a$ (nm)	$O_s$ (nm <sup>-1</sup> )	Asym
D2O	6.50	1.31	5.18	0.316	1.03
dSDS	6.50	1.32	5.17	0.308	1.00
+41months	5.90	1.52	4.37	0.327	0.96
dC16TAB	5.80	1.26	4.53	0.314	0.91
dC12E6	6.30	1.31	4.98	0.319	1.00
+41months	6.50	1.45	5.04	0.332	1.08
NaOD	5.80	1.24	4.55	0.311	0.90
+41months	6.40	1.06	5.33	0.368	1.18
11% D2SO4	6.40	1.81	4.58	0.282	0.90
+41months	7.40	1.16	6.24	0.324	1.20
33% D2SO4	11.4	2.56	8.83	0.166	0.95

**Table 4.** Summary of the structural data derived from correlation function analysis. Key:  $L$  = Long Period,  $l_c$  = average thickness of crystalline region,  $l_a$  = average thickness of amorphous region,  $O_s$  = specific inner surface, Asym =  $(O_s/2) \times L$  = asymmetry of distribution of nearest-neighbour spacings [38].

It should be noted that the correlation function for a system of crystallinity  $\omega_c$  is identical with that for a system of crystallinity  $(1 - \omega_c)$  because the two cases are mathematically equivalent (by virtue of Babinet's Theorem). Since the *CORFUNC* program has no *a priori* way of knowing whether  $\omega_c < 0.5$  or  $\omega_c > 0.5$  in a given system it is necessary to interpret its output in the light of any other known information. In the present case it was judged that the program had correctly assigned  $l_c$ ,  $\phi_c$ , and  $\omega_c$  to the right (i.e. crystalline) phase. The basis for this judgement is that  $l_c$  is close to the dimension of the monoclinic

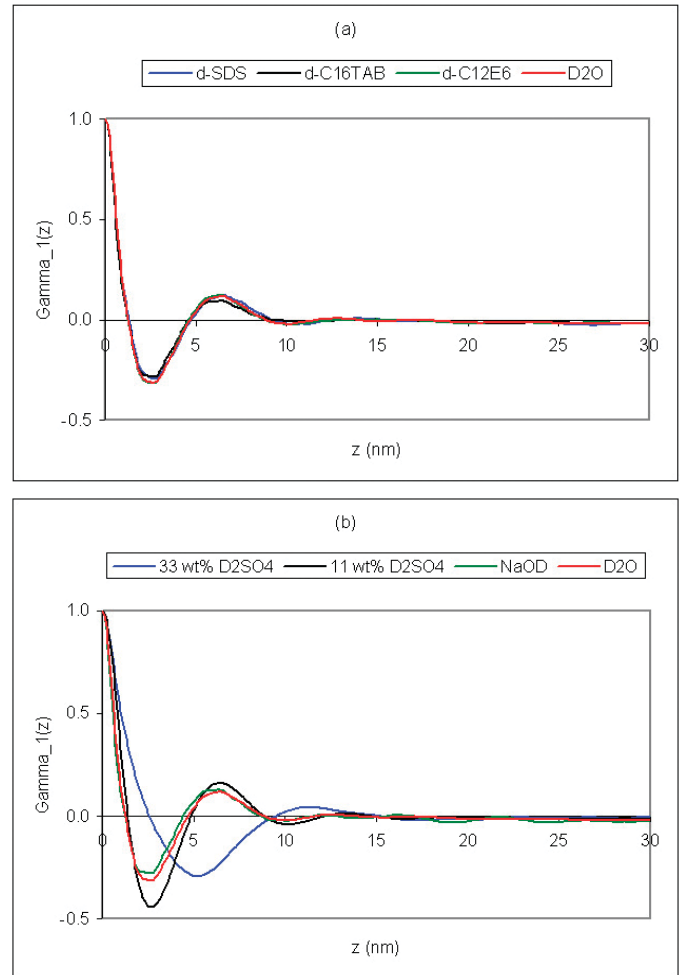


**Figure 10.** The correlation functions calculated from the 1D small-angle scattering data such as that shown in Figures 6, 8 and 9. (a) D<sub>2</sub>O and surfactant solutions. (b) Acid and alkali solutions.

Treated with:	$\phi_c$	$\omega_c$	$\phi_{sol}$	$10^{-21} Q^*$ (cm <sup>-4</sup> )	$10^{-29} E$ (cm <sup>-5</sup> )
D2O	0.207	0.202	0.690	4.492	0.241
dSDS	0.204	0.203	0.618	3.549	0.164
+41months	0.249	0.258	0.252	0.604	0.029
dC16TAB	0.198	0.217	0.717	4.582	0.226
dC12E6	0.209	0.207	>1	12.29	0.208
+41months	0.241	0.224	0.189	0.324	0.014
NaOD	0.194	0.215	0.342	0.963	0.056
+41months	0.196	0.166	0.269	0.616	0.053
11% D2SO4	0.257	0.284	0.533	2.953	0.195
+41months	0.188	0.157	0.522	2.430	0.109
33% D2SO4	0.213	0.224	n/a	n/a	0.208

**Table 5.** Summary of the physical data derived from correlation function and invariant analysis. Key:  $\phi_c$  = volume crystallinity,  $\omega_c$  = local crystallinity,  $\phi_{sol}$  = volume fraction of solvent in amorphous regions,  $Q^*$  = measured invariant integral ( $-1.5 < Q$  (nm<sup>-1</sup>)  $< 1.5$ ),  $E$  = Porod constant.

unit cell ( $c \sim 1.72$  nm), and  $\phi_c$  and  $\omega_c$  are more in keeping with expected crystallinities.

Inspection of the 2D small-angle diffraction patterns reveals them to be anisotropic, see Figure 11.

When the integrated intensity in the Bragg peak is plotted against azimuthal angle a distinct four-peak pattern emerges, evidence of biaxial alignment in the fibres (Figure 12).

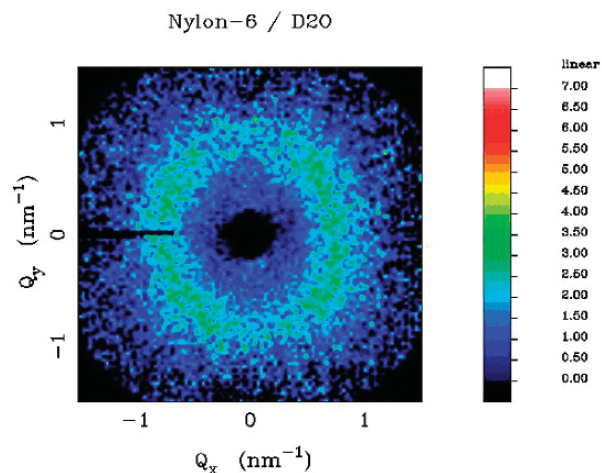


**Figure 11.** The 2D small-angle scattering from static fibres hydrated with D<sub>2</sub>O. The data have had a  $Q^{-3.9}$  power law background subtracted. The feature cutting across the left side of the pattern at  $Q_y = 0$  is an artefact of the way the image was processed. The slight tilt of the pattern is a consequence of poor sample mounting.

This alignment would have been imparted during the manufacturing process. Significantly the scattering patterns for fibres treated with NaOD and 33 wt% D<sub>2</sub>SO<sub>4</sub> do not show this feature.

It is quite clear that exposure of the fibres to water, the surfactant solutions, and even dilute acid, has negligible effect on this inherent alignment. In contrast, concentrated acid and alkali have a marked effect; the four-point pattern becomes a two-point pattern. The significant differences in overall scattering between fibres treated with water and 33 wt% D<sub>2</sub>SO<sub>4</sub> have already been remarked on, but curiously there are no obvious and equivalent differences in the scattering from fibres treated with NaOD.

## Summary and Conclusions

Small-Angle Neutron Scattering has been used to probe for changes in the microstructure of nylon fibres following exposure to concentrated surfactant, acid and alkali solutions.

The data are capable of differentiating between untreated and treated fibres.

In respect of exposure to surfactant solutions, there do not appear to be any untoward *chemical* consequences, though the cationic surfactant appears to be more effective at keeping the amorphous regions hydrated than either the anionic or non-ionic surfactants. This is in qualitative agreement with the observations of Frank [5].

It remains to be seen if there are any *mechanical* consequences. These might arise, for example, from surfactant crystallites that have penetrated into the core yarns "sawing" through the fibres, or by "connecting" adjacent fibres and thereby reducing the fibre redundancy that contributes to the load handling capability. Further work to address some of these outstanding issues is already in progress.

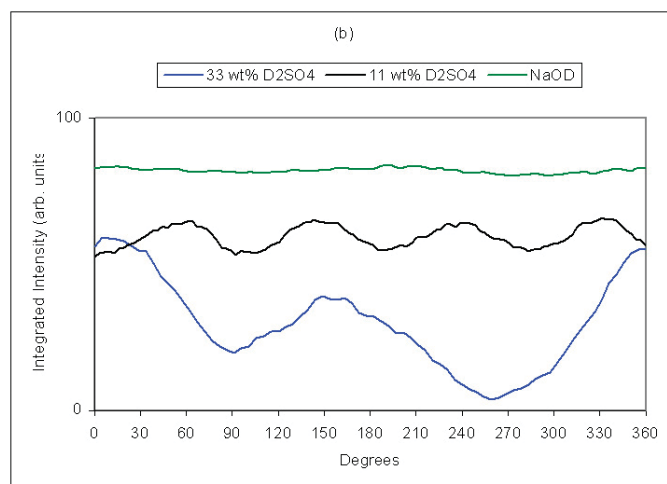
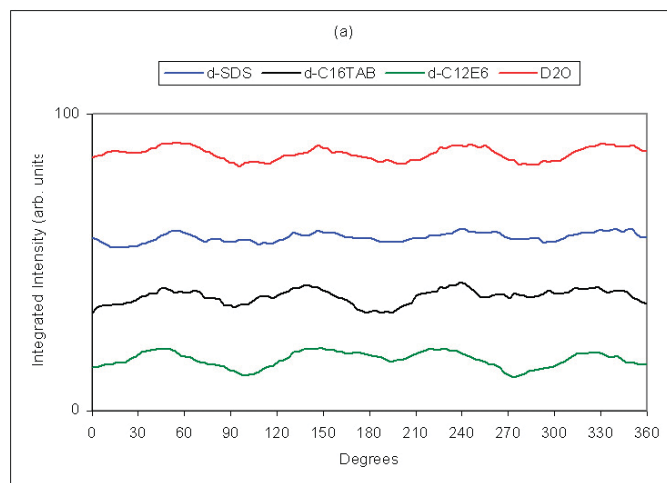


**Figure 12.** The (exponentially smoothed) integrated intensity in the Bragg peak. (a) Static fibres hydrated with D<sub>2</sub>O and surfactant solutions. (b) Static fibres hydrated with acid and alkali solutions. With the exception of the D<sub>2</sub>O curve in (a), the curves have been displaced vertically to aid clarity. The artefact in Figure 11 has been removed from these data.

One striking observation is just how robust the fibres are to acid hydrolysis. The degree of microstructural perturbation after 41 months in 1/3-strength car battery acid is really quite small, though more concentrated acid solutions degrade the fibres rather rapidly.

Additional diffraction measurements, and mechanical tests on the same samples, are already underway and will be reported in the near future.

## Acknowledgements

An oral contribution ("Hanging by a Thread") based on the subject matter of this paper was delivered at the 10<sup>th</sup> Annual CCP13 Fibre Diffraction and Non-Crystalline Diffraction Workshop in Stirling, Scotland, 13-15 June 2001.

The routine to convert LOQ reduced data files in ASCII format into BSL was written by J. Günter Grossmann at the Daresbury Synchrotron Radiation Source. It is now incorporated into the XCONV program in the CCP13 program suite.

The chemical structure diagrams are taken from the Macrogalleria at [www.psrc.usm.edu/macrog/index.htm](http://www.psrc.usm.edu/macrog/index.htm).

## References

- [1] Kaimin, I.F., Apinis, A.P., Galvanovskii, A.Ya. (1975) *Vysokomol. Soedin.*, **A17**, 41.
- [2] Inoue, K., Hoshino, S. (1976) *J. Polym. Sci., Polym. Phys. Ed.*, **14**, 1513.
- [3] Reimschuessel, H.K. (1978) Relationships on the effect of water on glass transition temperature and Young's modulus of nylon 6. *J. Polym. Sci., Polym. Chem. Ed.*, **16**, 1229-1236.
- [4] Smith, B. (1988) Effects of Rope Aging. *NSS News, Journal of the National Speleological Society of America*.
- [5] Frank, J.A. (1989) Fabric Softener and Rescue Rope. *Nylon Highway*.
- [6] Mark, J.E. (1999) *Polymer Data Handbook*. Oxford University Press.
- [7] Samon, J.M., Schultz, J.M., Hsiao, B.S. (2002) Structure development in the early stages of crystallisation during melt spinning. *Polymer*, **43**, 1873-1875.
- [8] Holmes, D.R., Bunn, C.W., Smith, D.J. (1955) *J. Polym. Sci.*, **17**, 159.
- [9] Arimoto, H., Ishibashi, M., Hirai, M., Chantani, Y. (1965) *J. Polym. Sci. Part A*, **3**, 317.
- [10] Salem, D., Weigmann, H., Polym. (1989) *Comm.*, **30**, 336.
- [11] Murthy, N.S., Curran, S.A., Aharoni, S.M., Minor, H. (1991) Premelting crystalline relaxations and phase transitions in nylon 6 and 6/6. *Macromol.*, **24**, 3215-3220.
- [12] Cooper, S.J., Atkins, E.D.T., Hill, M.J. (1998) Temperature-induced changes in lamellar crystals of monodisperse nylon 6 and nylon 6/6 oligoamides. *Macromol.*, **31**, 8947-8956.
- [13] Sikorski, P., Jones, N.A., Atkins, E.D.T., Hill, M.A. (2001) Measurement of the intersheet shear along the chain axis in nylon 6. *Macromol.*, **34**, 1673-1676.
- [14] Ramesh, C., Bhoje Gowd, E. (2001) High-temperature X-ray diffraction studies on the crystalline transitions in the a- and g- forms of nylon-6. *Macromol.*, **34**, 3308-3313.
- [15] Murthy, N.S., Minor, H., Bednarczyk, C., Krimm, S. (1993) Structure of the amorphous phase in oriented polymers. *Macromol.*, **26**, 1712-1721.
- [16] Zhang, Q.-X., Fu, P.-P., Zhang, H.-F., Mo, Z.-S. (2002) Microstructure analysis of nylon 66 by WAXD and SAXS. *Chem. Res. Chinese Uni.*, **18**, 358-363.
- [17] Wu, J., Schultz, J.M. (2002) Calculation of mesophase percentage of polymer fibres from 2D wide-angle X-ray scattering patterns. *Polymer*, **43**, 6695-6700.
- [18] Roldan, L.G., Kaufman, H.S. (1963) *J. Polym. Sci., Polym. Lett.*, **1**, 603.
- [19] Matyi, R.J., Crist, B. (1978) Small-angle X-ray scattering by nylon-6. *J. Polym. Sci., Polym. Phys. Ed.*, **16**, 1329-1354.
- [20] Rieger, J. (2002) Use of scattering methods in chemical industry - SAXS and SANS from fibers and films. Chapter 21, *Neutrons, X-rays and Light: Scattering Methods Applied to Soft Condensed Matter*, Lindner, P., Zemb, Th. (editors), North-Holland.
- [21] Murthy, N.S., Stamm, M., Sibilica, J.P., Krimm, S. (1989) Structural changes accompanying hydration in nylon-6. *Macromol.*, **22**, 1261-1267.
- [22] Murthy, N.S., Orts, W.J. (1994) Hydration in semicrystalline polymers: small-angle neutron scattering studies of the effect of drawing in nylon-6 fibres. *J. Polym. Sci. Part B*, **32**, 2695-2703.
- [23] Papanek, P., Fischer, J.E., Murthy, N.S. (2002) Low-frequency amide modes in different hydrogen-bonded forms of nylon-6 studied by inelastic neutron scattering and density-functional calculations. *Macromol.*, **35**, 4715-4182.
- [24] Hutchinson, J.L., Murthy, N.S., Samulski, E.T. (1996) Deuterium nmr studies of water in oriented nylon-6 fibres. *Macromol.*, **29**, 5551-5557.
- [25] Murthy, N.S., Akkapeddi, M.K., Orts, W.J. (1998) Analysis of lamellar structure in semicrystalline polymers by studying the absorption of water and ethylene glycol in nylons using small-angle neutron scattering. *Macromol.*, **31**, 142-152.
- [26] Plestil, J., Baldrian, J., Ostanevich, Yu.M., Bezzabotnov, V.Y. (1991) Small-angle neutron and X-ray scattering study of swollen nylon-6. *J. Polym. Sci. Part B*, **29**, 509-514.
- [27] Crawshaw, J., Vickers, M.E., Briggs, N.P., Heenan, R.K., Cameron, R.E. (2000) The hydration of TENCEL cellulose fibres studied using contrast variation in small angle neutron scattering. *Polymer*, **41**, 1873-1881.
- [28] [www.isis.rl.ac.uk](http://www.isis.rl.ac.uk)
- [29] [www.isis.rl.ac.uk/LargeScale/LOQ/LOQ.htm](http://www.isis.rl.ac.uk/LargeScale/LOQ/LOQ.htm)
- [30] King, S.M., Heenan, R.K. Using COLETTE. RAL Report RAL-95-005, Rutherford Appleton Laboratory (1995).
- [31] Wignall, G.D., Bates, F.S. *J. Appl. Cryst.*, **20**, 28-40 (1987).
- [32] [www.ccp13.ac.uk](http://www.ccp13.ac.uk)
- [33] Kotlarchyk, M., Ritzau, S.M. (1991) Paracrystal model of the high-temperature lamellar phase of a ternary microemulsion system. *J. Appl. Cryst.*, **24**, 753-758.
- [34] Heenan, R.K. (1989) "FISH" Data Analysis Program. RAL Report RAL-89-129, Rutherford Appleton Laboratory. Also see: [www.isis.rl.ac.uk/LargeScale/LOQ/FISH/FISH\\_intro.htm](http://www.isis.rl.ac.uk/LargeScale/LOQ/FISH/FISH_intro.htm)
- [35] Strobl, G.R., Schneider, M. (1980) Direct evaluation of the electron density correlation function of partially crystalline polymers. *J. Polym. Sci., Polym. Phys. Ed.*, **18**, 1343-1359.
- [36] Li, L., Koch, M.H., de Jeu, W.H. (2003) Crystalline structure and morphology in nylon-12: A small- and wide-angle X-ray scattering study. *Macromol.*, **36**, 1626-1632.
- [37] Koberstein, J., Stein, R.J. J. (1983) *Polym. Sci., Polym. Phys. Ed.*, **21**, 2181-2200.
- [38] Strobl, G.R., Schneider, M.J., Voigt-Martin, I.G. (1980) Model of partial crystallisation and melting derived from small-angle X-ray scattering and electron microscopic studies on low-density polyethylene. *J. Polym. Sci., Polym. Phys. Ed.*, **18**, 1361-1381.